ACS APPLIED MATERIALS & INTERFACES

Research Article

www.acsami.org

Unraveling the Adsorption Mechanism of Mono- and Diaromatics in Faujasite Zeolite

Huimin Zheng,[†,§] Liang Zhao,*[,†,§] Jingjing Ji,[†] Jinsen Gao,[†] Chunming Xu,[†] and Francis Luck[‡]

[†]State Key Laboratory of Heavy Oil Processing, China University of Petroleum (Beijing), 18 Fuxue Road, Beijing 102249, China

[‡]Scientific Development Division, TOTAL S.A., 24 Cours Michelet, 92069 Cedex Paris La Defense, France

Supporting Information

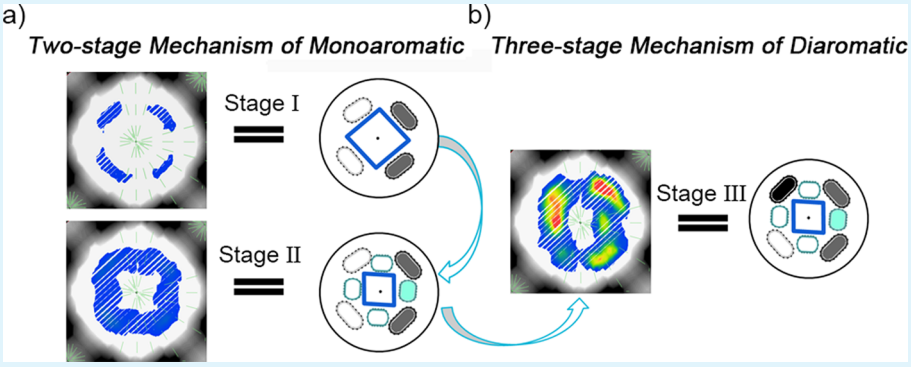

ABSTRACT: Monte Carlo simulations are performed to study the adsorption of aromatic molecules (toluene, styrene, *o*-xylene, *m*-xylene, *p*-xylene, 1,3,5-trimethylbenzene, and naphthalene) in all-silica faujasite (FAU) zeolite. For monoaromatics, a two-stage "ideal adsorption" and "insertion adsorption" mechanism is found by careful inspection of locations and distributions of the adsorbed toluene molecules. The validity of this mechanism is confirmed for all monoaromatics considered in the current study. Remarkably, the number of C atoms per unit cell corresponding to the inflection point of adsorbate loading ($C_{I\text{-}P}$) is defined as a valid and convenient characterizing factor in the packing efficiency of monoaromatics in the FAU zeolite. For the case of naphthalene, a type of diaromatic, the three-stage mechanism is proposed, which consists of the first two stages and a third stage of "overideal adsorption". The so-called overideal adsorption is labeled because the naphthalene molecules start to occupy the S site nonideally at loadings that approach saturation, leading to a more localized feature of the adsorbates. The explicit adsorption mechanism can be used to understand the loading dependence of isosteric adsorption heat for the aromatics concerned.

KEYWORDS: *aromatics, FAU zeolite, adsorption, Monte Carlo simulation*

1. INTRODUCTION

Faujasite (FAU) zeolites are used extensively in practical applications such as adsorption, separation, and catalysis, especially in the oil refining and petrochemical industries, mainly because of their high surface area, high hydrothermal stability, and appropriate acidity.[1,2] In these applications, a good knowledge of adsorption of adsorbates inside FAU zeolites is a prerequisite for clarifying the underlying mechanism of these processes as well as exploring further applications of the zeolites.[3,4] With regard to the active research in the loading dependence of selectivity[5,6] and diffusivity[7] of aromatics in FAU zeolites, a thorough understanding of adsorption mechanisms at all loadings could shed light on the molecular origin of the change of adsorption and diffusion behaviors.

In contrast to the growing body of data related to adsorption and diffusion of aromatics in zeolites at dilute loading, such as benzene,[8] toluene,[9] xylene,[10] and 1,3,5-trimethylbenzene (TMB),[6] the research on the adsorption mechanism of important aromatics at high loadings in zeolites requires more attention. Limited information is available on the entire loading range in the same materials. The complexity of the system can increase significantly when pore filling approaches saturation values.[6,11] For example, anomalous adsorption behavior of cyclic hydrocarbons (benzene, *p*-xylene, and others) has been reported in silicalite-1 at high adsorbate loadings.[12]

Recently, our studies on the benzene/HY system revealed an intriguing change of adsorption mechanism with increased loading and demonstrated that understanding of the adsorption mechanism from the molecule level is highly necessary.[13] A two-stage adsorption mechanism was proposed for benzene in HY zeolite for loadings below and above an inflection point of loading (labeled I-P) regardless of the Al content (Si/Al = 3.3−∞). Therefore, the adsorption mechanism is likely to change with loading for accessible aromatics such as branched monoaromatics and diaromatics in FAU zeolite based on the

Received: January 14, 2015
Accepted: April 24, 2015
Published: April 24, 2015

DOI: 10.1021/acsami.5b00399
ACS Appl. Mater. Interfaces 2015, 7, 10190−10200

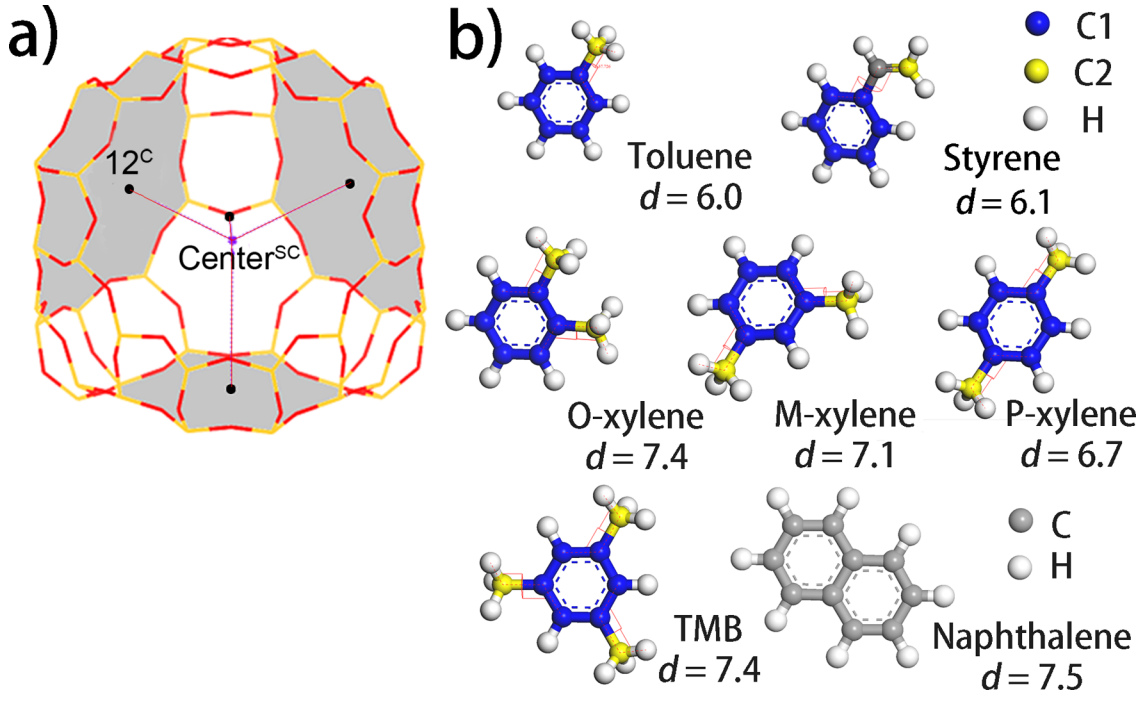

Figure 1. (a) One SC of FAU. The positions of 12^C and $center^{SC}$ are shown by black and purple dots, respectively. (b) Models of all adsorbates. Kinetic diameters (d) of toluene,[17] styrene,[18] *o*-, *m*-, *p*-xylene,[17] TMB,[17,19,20] and naphthalene[21] are shown in angstroms.

close analogies in their structures. In addition, compared with small pore zeolites, i.e., mordenites, catalysts containing zeolite Y with large pore supercages (SCs) tend to produce more branched aromatics.[14] Clarifying whether an adsorption mechanism exists that is universally applicable in FAU zeolites can shed light on the separation and catalysis processes, which are of interest to industries that generally use different types of aromatics.

This work further explores the adsorption mechanisms of aromatics: toluene, styrene, *o*-, *m*-, and *p*-xylene, TMB, and naphthalene on siliceous FAU zeolite by force-field-based Monte Carlo (MC) simulations, with a focus on evaluating the size-related packing effects of FAU zeolite, if any, on the loading dependence of the adsorption mechanism.

2. MODELS AND METHODS

The framework of FAU zeolite was shown in a neutron diffraction study conducted by Fitch et al.,[15] which has a cubic unit cell with cell length a = 24.8536 Å. The accessible space for aromatic molecules was the SC with a diameter of ~13 Å formed by sodalite cages, as shown in Figure 1a. Each of two SCs was connected by a 12-membered window (12-T ring) with a diameter of ~7.4 Å. Then, the centers of the SC and 12-T ring were abbreviated to $center^{SC}$ and 12^C, respectively. For branch adsorbates, toluene, styrene, xylenes, and TMB, the ring C atoms are labeled C1 (blue) and the C atoms at the end of the branch are labeled C2 (yellow). The crystallographic unit cell consisting of eight SCs was used in this simulation because no size effect has been noticed for the systems in this study.[16] The previous finding was that for benzene in HY zeolite, the two-stage adsorption mechanism generally existed for all Si:Al from 2.43 to ∞.[13] Therefore, only siliceous FAU zeolite (labeled S-0) was relevant for aromatic adsorbates in this study.

As is well-known, the kinetic diameter is the smallest diameter that allows the gas molecule to enter the inner cavity (SC in this case).[22] Thus, the largest adsorbate employed in the present study was naphthalene, which had a kinetic diameter comparable with the size of the 12-T ring. Aromatic molecules with a substantial difference in carbon number (CN = 6−10), kinetic diameter (d = 6−7.5 Å), and shape (see Figure 1b) were chosen to reveal the influence of molecular dimensions on the loading-dependent adsorption mechanism.

Commercial software Materials Studio from Accelrys Inc. was used for geometry optimization and MC simulations. The COMPASS force field,[23] which has been successfully applied to explore the adsorption of many adsorbate/zeolite systems,[12,24−30] including the aromatics in FAU zeolite,[31] was used to define the interactions between the atoms. The partial charges of Si and O atoms were obtained from ref 32, in which the authors there placed their values on the reasonable middle ground between simplicity of the charge description and validity of the local environment. For adsorbates, the charges implemented in COMPASS force field were used for monoaromatics, and the charges of naphthalene were taken from ref 33. The same with most common charges for the C atoms of monoaromatics, the methyl group C atoms, unsubstituted ring C atoms, and substituted ring C atoms were charged differently. More information on partial charges is provided in the Supporting Information(Table SI1 and Figures SI1 and SI2).

The simulation scheme employed in this study is summarized briefly as follows. First, the structures of aromatic molecules shown in Figure 1b and the S-0 model were optimized by Smart minimizer method.[16,34] Second, adsorption isotherms were computed using grand-canonical ensemble MC (GCMC) consisting of 4×10^7 equilibration and 4×10^7 production steps. In this study, one MC step is defined as the attempt to move each adsorbate molecule once. In each step, trial movement was randomly selected with a fixed probability: guest molecule translation of 20%, guest molecule rotation of 20%, guest molecule exchange (sum of the ratios of the creation and deletion steps with equal weighing) of 55%, and guest molecule regrowth of 15%.

Then, MC simulations in the canonical ensemble were conducted for aromatics in S-0 at 298 K. The fixed loading simulations were performed for loadings from one molecule per unit cell (molecule/UC) to saturation concentrations, that is, 40, 36, 36, 36, 34, 30, and 28 molecules/UC for toluene, styrene, *o*-xylene, *m*-xylene, and *p*-xylene, naphthalene, and TMB. The equilibration MC steps were 1×10^7 followed by another 1×10^7 MC steps for production. Several loading points of our simulations were recomputed with more MC steps and affirmed the convergence of our simulations. To obtain accurate distribution properties of adsorbates, 1×10^5 configuration frames were saved. The metropolis[16] and configurational bias techniques were

DOI: 10.1021/acsami.5b00399
ACS Appl. Mater. Interfaces 2015, 7, 10190−10200

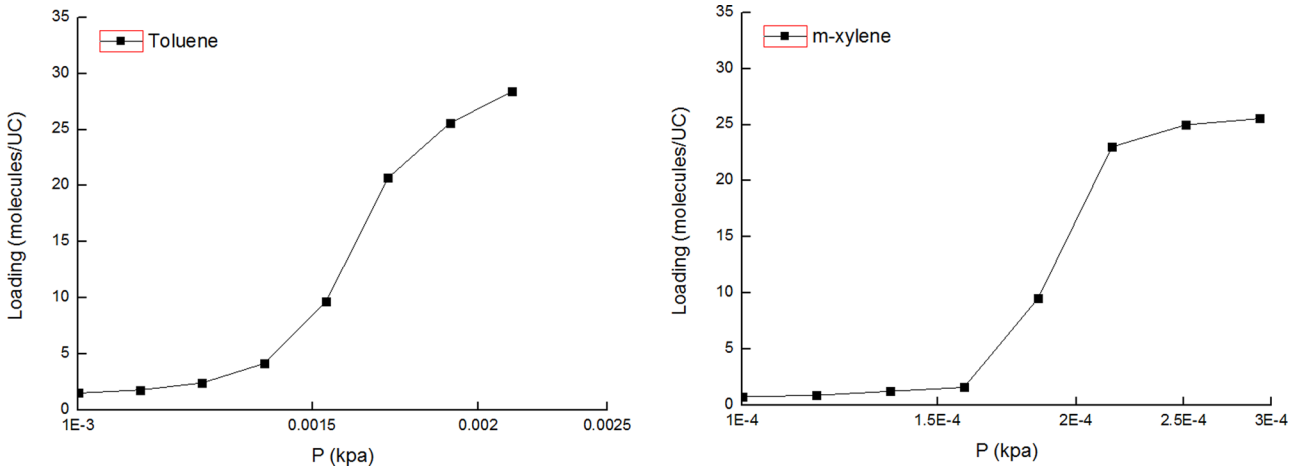

Figure 2. Toluene (squares) and *m*-xylene (diamonds) adsorption isotherms in 0Al model at 298 K (where, for example, 1E-4 represents 1×10^{-4}).

used for naphthalene and branched aromatics (toluene, styrene, *o*-, *m*-, and *p*-xylene, and TMB),[35] respectively. Aromatic molecules can switch between SCs freely rather than being stuck in one SC in the simulations showing that the systems were well-equilibrated and the adsorbates were sampled representatively, as illustrated in Figures SI3 and SI4, Supporting Information. The electrostatic potential energy was calculated by the Ewald summation method[36,37] with a calculation accuracy of 4.184 J/mol. The cutoff distance for the calculation of the van der Waals potential energy was set as 12 Å.[38] The periodic boundary conditions were applied in the three coordinate directions.[39]

3. RESULTS AND DISCUSSION

3.1. Adsorption Isotherms. The properties of adsorption isotherms are important for understanding the adsorption behavior of adsorbates in micropores. Figure 2 shows the adsorption isotherms developed for the first time for toluene and *o*-xylene on the 0Al model at 298 K. Interestingly, both adsorbates exhibit an inflection point, in which the curvature changes from positive (increasing slope) to negative (decreasing slope). This observation is similar to experimental results reported by Zeng et al.[8] and Takahashi et al.[40] for benzene in an all-silica FAU system and should be related to the fact that the adsorption mechanism changes with the ressure (loading) of benzene. In order to further explore the effect of size-related packing on adsorption mechanisms, the spatial distributions of aromatics on the 0Al model need to be carefully examined.

3.2. Relative Concentration. The relative concentration plots, $P(x)$, of the center of mass (COM) of toluene, styrene, *o*-, *m*-, and *p*-xylene, TMB, and naphthalene along the *x*-direction of the zeolite models are illustrated in Figure 3. In the case of monoaromatics, from infinite dilution up to 32, 28, 28, and 24 molecules/UC for toluene, styrene, *o*-, *m*-, and *p*-xylene, and TMB, respectively, $P(x)$ exhibits identical distributing curves, indicating that the adsorption sites revealed at infinite dilution remain unchanged in the vast majority of loadings. At this stage, the adsorption mechanism clearly belongs to "ideal adsorption," referring to adsorbates ideally located on the adsorption sites. However, at higher loadings (corresponding curves are colored red in Figure 3), $P(x)$ changes obviously, representing a change of adsorption behavior compared with lower loadings. This condition strongly suggested the change of the adsorption mechanism separated by an I-P.

This finding resembles a previous observation on benzene in HY zeolites.[13] That is, from infinite dilution up to ~32 molecules/UC, the feature of $P(x)$ is scarcely influenced by benzene loading, following the ideal adsorption mechanism. However, at higher loadings, an "insertion adsorption" mechanism was demonstrated, which represented benzene molecules inserting into the space between existing adsorbed molecules (occupying IN sites) with no obvious rearrangement for previously adsorbed molecules.[13] Based on the similarity of the loading dependence of $P(x)$ of monoaromatics in FAU zeolite, and the close analogies between their structures, the two-stage "ideal and insertion" adsorption mechanism can likely explain the anomalous adsorption behavior in all of these systems, which is possible with other monoaromatics. Meanwhile, $P(x)$ exhibits a more complex trend for naphthalene compared with monoaromatics, and the adsorption behavior seems to change twice at low (3 molecules/UC) and high (24 molecules/UC) loadings, respectively. Therefore, the branched monoaromatics and naphthalene are illustrated separately hereafter. Toluene is chosen as the example of the first case and is discussed in greater detail as follows.

3.3. Monoaromatics. Generally, the following possible distributions exist for aromatics in cage-like FAU zeolite: (a) ideal adsorption, in which adsorbed benzene molecules are located ideally on the adsorption site near the SC surface (S site); (b) insertion adsorption, in which adsorbed benzene molecules keep their original positions and the later one is inserted into the space between the adsorbed ones; (c) rearrangement adsorption, in which the later benzene significantly affects the distribution of the adsorbed adsorbates. So far, the first case is strongly rejected by the $P(x)$ data in Figure 3. For the second stage, the explicit adsorption mechanism can be obtained based on the radial distribution functions (RDFs) of toluene in Figure 4.

As shown in Figure 4a, the RDFs of COM−COM are consistent with those of benzene.[13] That is, the main peaks stay in the same position over the entire loading range, which represents molecules that occupy preferentially S sites. This condition clearly rules out the possibility of rearrangement involving collective participation of the majority of the toluenes in the second stage, which is generally characterized by a shorter distance between adsorbates. The new peaks at approximately 4.5 and 7.8 Å, which represent toluene molecules that disobey the ideal adsorption mechanism, appear in Figure 4a at loadings above the I-P. Furthermore, the first peak of RDFs between C2 atoms of toluene (C2−C2) in Figure 4b increases significantly at loadings above the I-P, in contrast with

DOI: 10.1021/acsami.5b00399
ACS Appl. Mater. Interfaces 2015, 7, 10190−10200

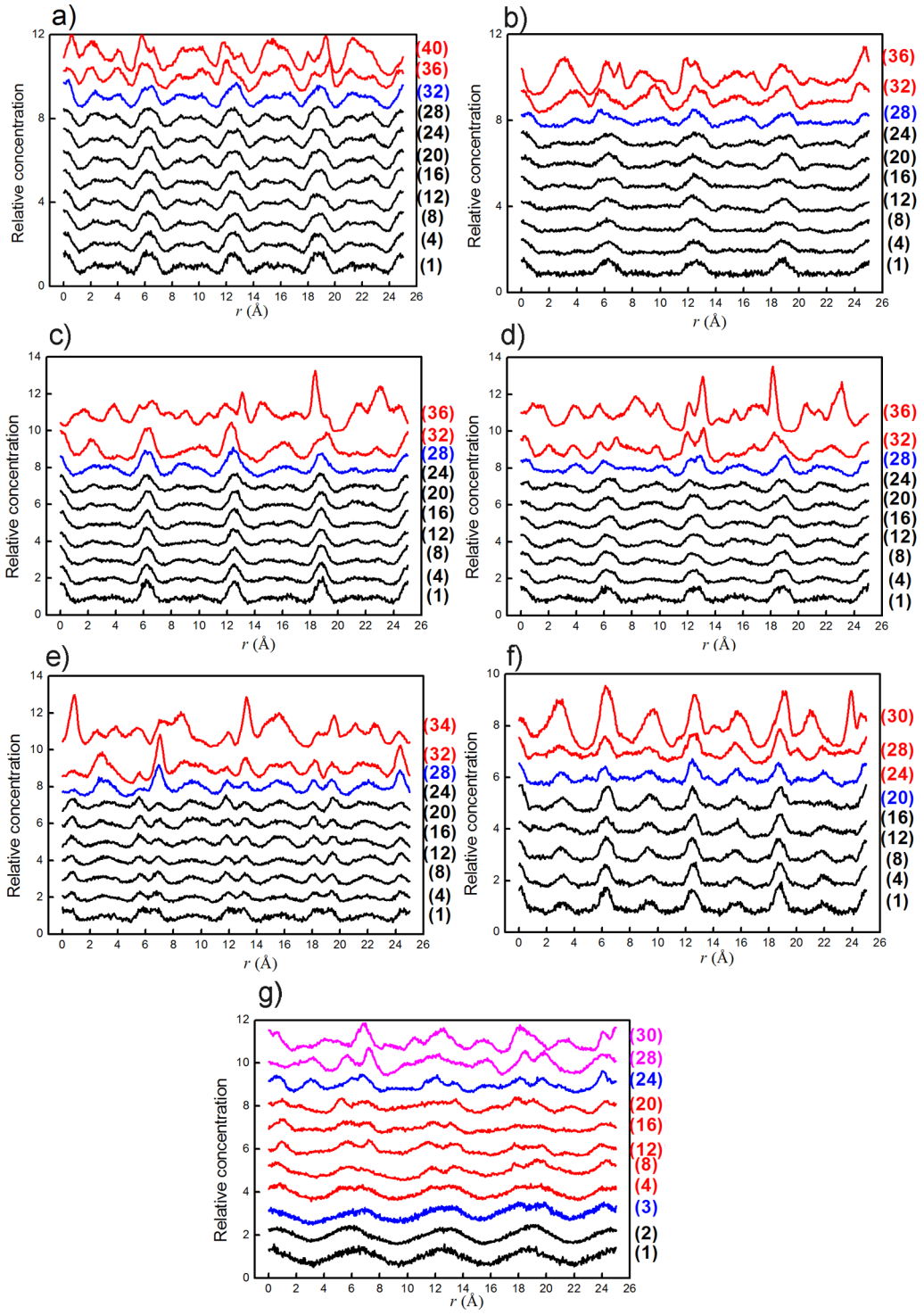

Figure 3. Relative concentration $P(x)$ of the COM at different loadings along the x-direction of the unit cell in the 0Al model for (a) toluene, (b) styrene, (c) *o*-xylene, (d) *m*-xylene, (e) *p*-xylene, (f) TMB, and (g) naphthalene. For the monoaromatics, black, blue, and red numbers given in the parentheses are loadings corresponding with the curves below, at, and above the I-P in molecules/UC. The revolution of $P(x)$ with loading is more complex and will be discussed separately.

the gradual decrease for loadings below the I-P. This result further supported the change of mechanism at the I-P for toluene. The first peak of COM−12^C in Figure 4c decreases as the loadings approach saturation, which indicates that the 12-T window becomes increasingly less occupied. Therefore, the new peaks at loadings above the I-P should not be attributed to an increased amount of toluene captured by the 12-T ring. This finding can be confirmed by the density contour in Figure 4d. As expected, the population in the 12-T ring first increases with loading because of saturation of energetically favorable S sites and increases in adsorbate−adsorbate interaction.[16] However, at loadings close to saturation status, the occupation of the 12-T ring decreases with loading and is accompanied by an interesting highly localized distribution inside the SC, which is

DOI: 10.1021/acsami.5b00399
ACS Appl. Mater. Interfaces 2015, 7, 10190−10200

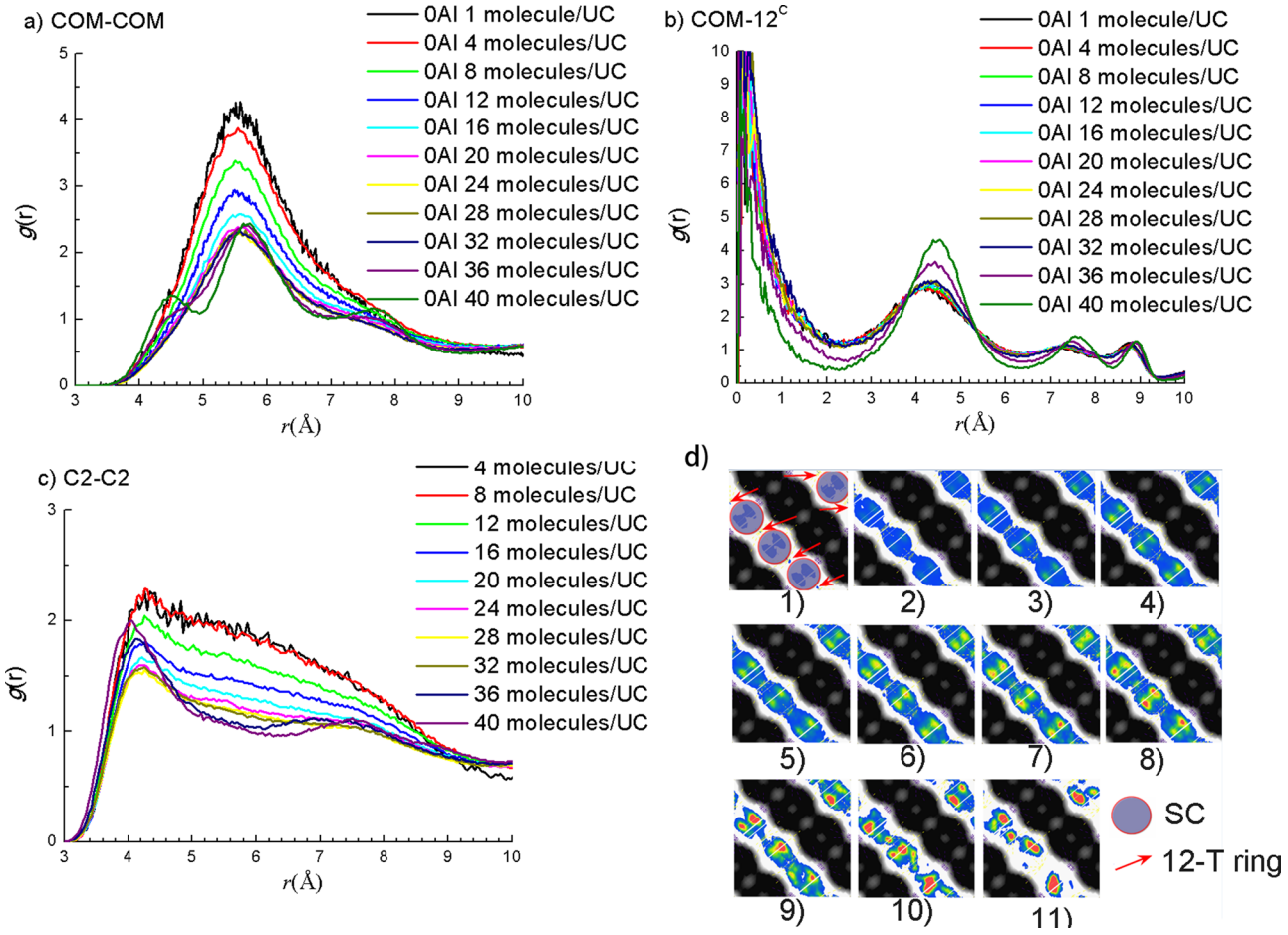

Figure 4. RDFs of (a) COM−COM, (b) C2−C2, and (c) COM−12^C of toluene at various loadings. (d) Density contours of toluene on 0Al, at loadings of (1) 1, (2) 4, (3) 8, (4) 12, (5) 16, (6) 20, (7) 24, (8) 28, (9) 32, (10) 36, and (11) 40 molecules/UC, respectively. Accessible and blocked places of the structure are shown as white and black. The unit of density scale is the number of adsorbate molecules per $Å^3$.

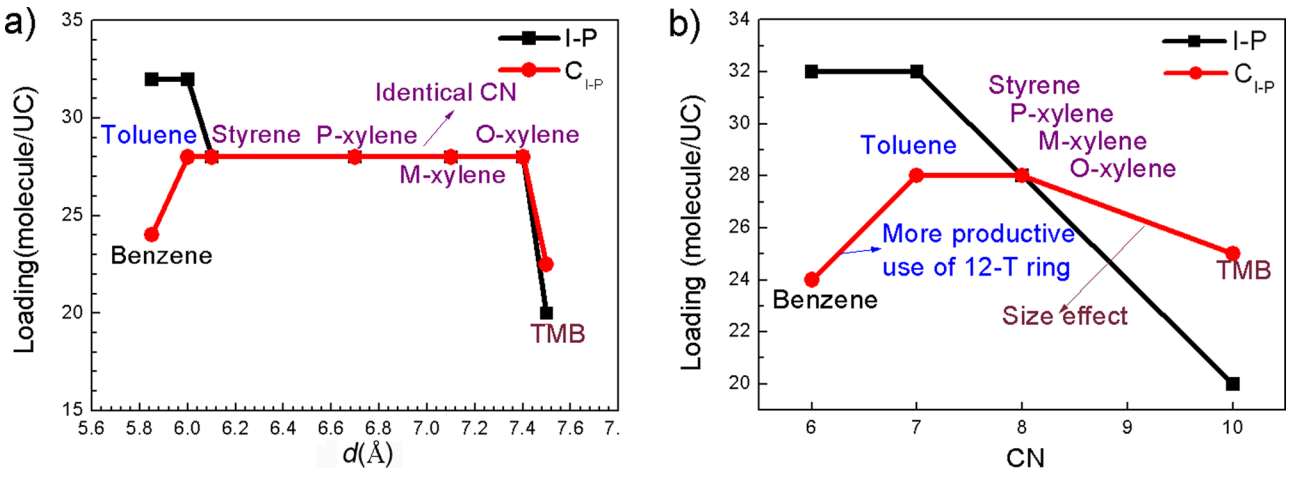

Figure 5. Adsorbate loading (I-P, black squares) and C atoms (C_{I-P}, red circles) that correspond with the I-P for monoaromatics versus (a) *d* and (b) CN of adsorbates.

the sign of increasing packing efficiency. Consequently, for loadings above the I-P, more toluene molecules have to fit into the SC and no influence on the fully occupied S sites is identified; i.e., the insertion adsorption mechanism at loadings above the I-P can be justified. Considering the adsorption behavior of all loadings, we obtain the adsorption mechanism for toluene/0Al, which is the same as the adsorption of the benzene/HY system.

Results for other monoaromatics are summarized in the Supporting Information. These adsorbates follow the same two-stage adsorption mechanism with I-P ranging between 20 and 28 molecules/UC. That is, the loading that corresponds with the I-P that reveals the packing efficiency of adsorbates, changes

DOI: 10.1021/acsami.5b00399
ACS Appl. Mater. Interfaces 2015, 7, 10190−10200

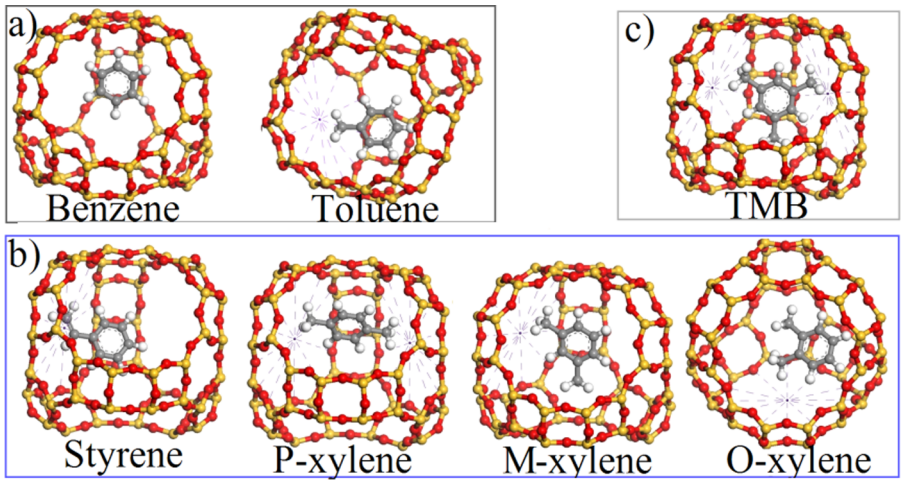

Figure 6. Representative snapshots of (a) small, (b) medium, and (c) large monoaromatics in the 0Al model at 1 molecule/UC. The dashed lines denote the 12^{C} of concerns.

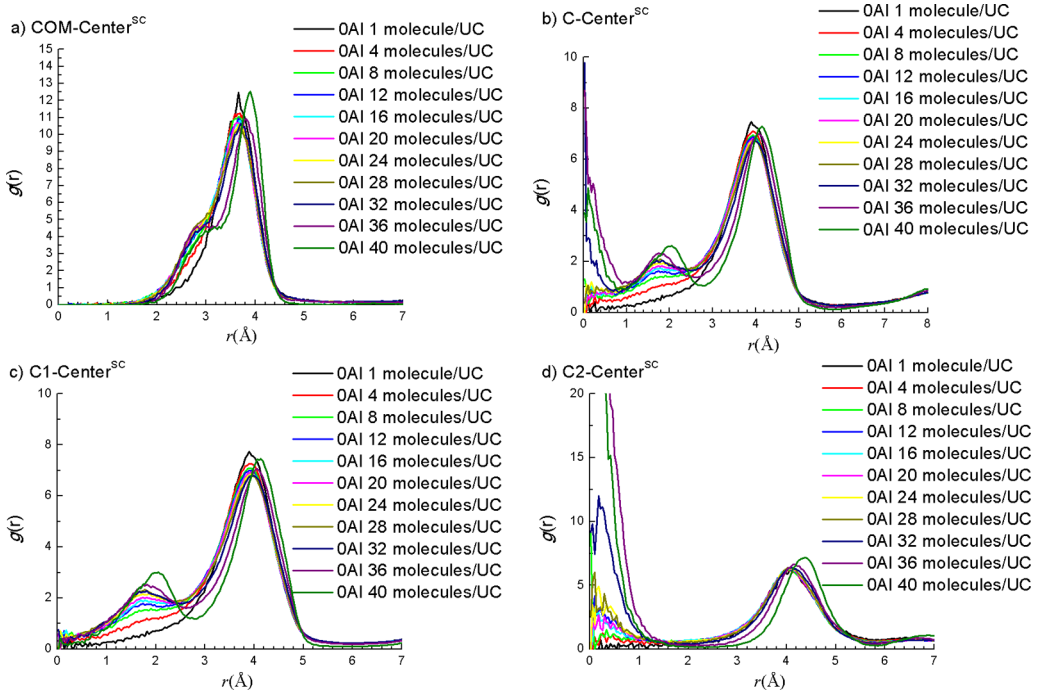

Figure 7. RDFs of (a) COM−center^{SC}, (b) C−center^{SC}, (c) C1−center^{SC}, and (d) C2−center^{SC} for toluene in 0Al at various loadings.

with the *d* and CN of adsorbates. Compared with the number of molecules per unit cell, the number of C atoms adsorbed per unit cell at the I-P ($C_{I\text{-}P}$) can detect the packing efficiency more accurately with regard to adsorbates that have different CNs. The change in molecule loading (black squares) and number of C atoms (red circles) that correspond to the I-P for monoaromatics with *d* and CN are shown in Figure 5a,b, respectively.

Based on the changing rule of packing efficiency with CN in Figure 5b, the adsorbates can be classified into three groups: small ($C < 8$), medium ($C = 8$), and large aromatics ($C > 8$), as shown in Figure 6. Interestingly, for aromatics in the first group (benzene and toluene), although the same I-P at 32 molecules/UC is presented, the $C_{I\text{-}P}$ of toluene is even larger than that of benzene. Our finding indicates more efficient packing of toluene since both benzene and toluene are able to fill >90% of the theoretically available pore volume of FAU with similar saturate loading.[6] This condition is caused by higher utilization of pore volume by the methyl group of toluene, which is able to approach the 12-T ring, as illustrated by representative low-energy snapshots in Figure 6.

For medium aromatics, being C8 (styrene and *p*-, *m*-, and *o*-xylene), the packing efficiency ($C_{I\text{-}P}$) is the same as that for toluene and scarcely dependent on *d*, revealing the ability of the branched groups of C8 aromatics to efficiently exploit the 12-T ring regardless of the shapes of the aromatics. However, a more bulky aromatic (TMB) can no longer maintain this packing efficiency ($C_{I\text{-}P}(TMB) < C_{I\text{-}P}(C8)$) by counteracting the size effect (additional methyl group) with the utilization of the 12-T ring. In addition, the packing efficiency of TMB is only slightly lower than that of benzene, which highlights the significant role of the 12-T ring in diminishing the size effect.

Evaluating the packing effect of $C_{I\text{-}P}$ from an explicit adsorption mechanism can consider both the size effect and

DOI: 10.1021/acsami.5b00399
ACS Appl. Mater. Interfaces 2015, 7, 10190−10200

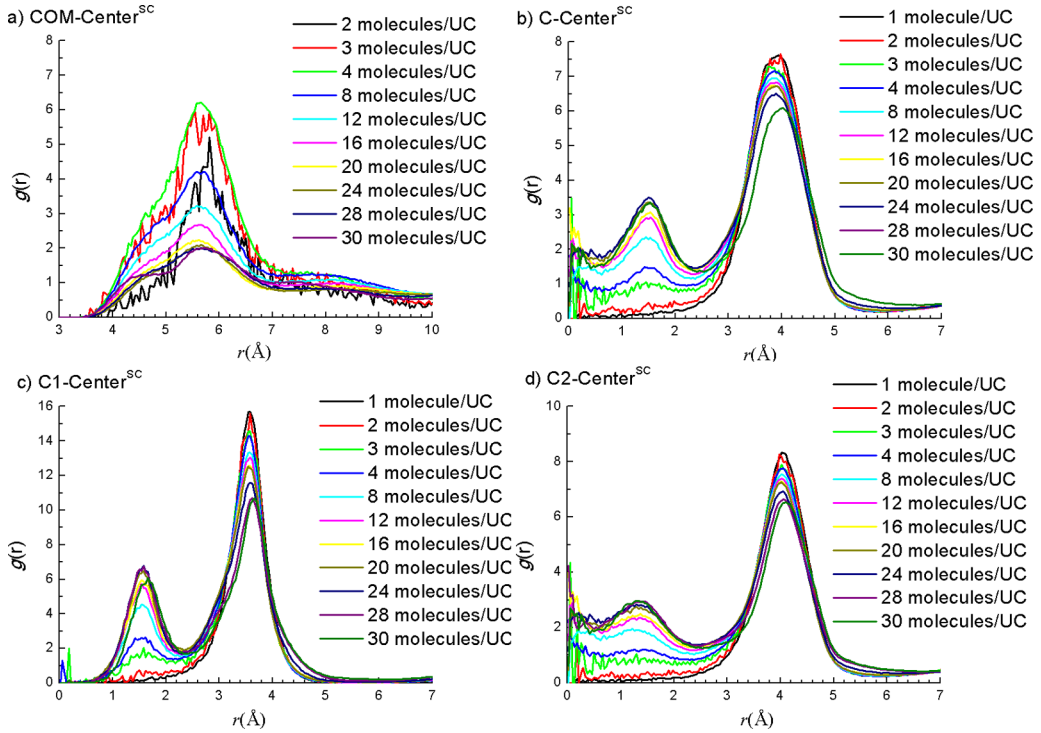

Figure 8. RDFs of (a) COM−center^{SC}, (b) C−center^{SC}, (c) C1−center^{SC}, and (d) C2−center^{SC} for naphthalene in 0Al at various loadings.

adsorption strength of aromatics. For example, an unexpected loading-dependent selectivity effect was observed in the adsorption of benzene/*p*-xylene mixtures on Na−X zeolite, which selectively adsorbs *p*-xylene at high benzene concentrations.[41] According to our findings, this condition is probably due to more efficient packing of *p*-xylene compared with that of benzene; i.e., $C_{I\text{-}P}$(benzene) < $C_{I\text{-}P}$(*p*-xylene).

Although the insertion mechanism is positively defined for monoaromatics, it is unclear whether the specified IN sites of adsorbents are near the center^{SC} as in the case of benzene. At first, the RDFs of COM−center^{SC} in Figure 7a are examined to clarify the insertion position of toluene in the SC of the zeolite framework. The population of toluene close to the center^{SC} is almost zero for all loadings, which is generally true for all of the adsorbates in this study, indicating that the center^{SC} is energetically highly unfavorable. At zero pore filling, the only peak shown at 3.7 Å corresponds with the adsorption on the S site, this peak gradually decreases, and its position is unaffected by loading under the I-P (32 molecules/UC). With increasing loadings, a gain in intensity of adsorption close to the cage center results in a shoulder at 2.5−3.0 Å that appears on the shorter distance side of the RDFs. Although no obvious change of the shoulder can be observed at loadings above the I-P, we believe that the toluene molecules are inserted in the position near the center^{SC}. The reason is that the position of the main peak shifts away from the center^{SC} (from 3.7 to 3.9 Å), which may be attributed to the inserted toluene that pushes molecule-occupied S sites to the surface of the zeolite framework.

The location of the inserted molecules can be further identified regarding the RDFs between C atoms and center^{SC} in Figure 7b−d. The C atoms of adsorbates are labeled C1 and C2, as illustrated in Figure 1b, to specify the relative position of the aromatic ring and the side chain. Several interesting observations can be made. Three peaks are observed at approximately 0, 1.9, and 3.9 Å for the RDFs of the *C*−center^{SC} in Figure 7b. The first peak of the *C*−center^{SC} at ∼0 Å corresponds to the first peak of the C2−center^{SC} shown in Figure 7d and is well-defined only at saturated loadings. Therefore, the first peak refers to the C2 atoms of the toluene following the insertion mechanism. The second peak of the *C*−center^{SC} corresponds to the first peak of the COM−center^{SC} and C1−center^{SC} shown in Figure 7a,c, which grows more intensely with loading and develops into a peak at loadings above the I-P, stemming from the C1 atoms of the toluene following the insertion mechanism. A similar trend is displayed for the RDFs of styrene, *o*-, *m*-, and *p*-xylene, and TMB (Supporting Information), which agreed well with the conclusion. The behavior of the RDFs suggests that the inserted monoaromatics are adsorbed near the center^{SC}, which is consistent with benzene. Moreover, the RDFs and low-energy snapshots of the inserted aromatics reveal that they adsorb with the head (benzene ring, C1) facing the framework and the tail (methyl side group C2) pointing to the center^{SC}.

3.4. Naphthalene. Figure 8 presents the RDFs of naphthalene with the zeolite at different loadings at 298 K. At the 2 molecules/UC, the RDF of COM−COM shown in Figure 8a is narrow, sharp, and unimodal with the peak maximum at ∼5.7 Å, which confirms that two naphthalenes are adsorbed ideally at low concentrations. In this case, the corresponding site is the S site characterized by the main peak in Figures 8b, 6c, and 5d. Starting from 3 molecules/UC, higher loadings of naphthalene result in a distinct shoulder peak at 4.3−5 Å in Figure 8a at the majority of the loadings (3−30 molecules/UC). Because the position of this new peak is an analogue of the peak that represents the inserted monoaromatics, the insertion mechanism expected for naphthalene starts from relatively low loadings. The RDFs in Figure 8b−d show a well-defined small peak at a position closer to the center^{SC} and confirm this anticipation. These results suggest that the naphthalene molecules tend to form a trimer in the SC

DOI: 10.1021/acsami.5b00399
ACS Appl. Mater. Interfaces 2015, 7, 10190−10200

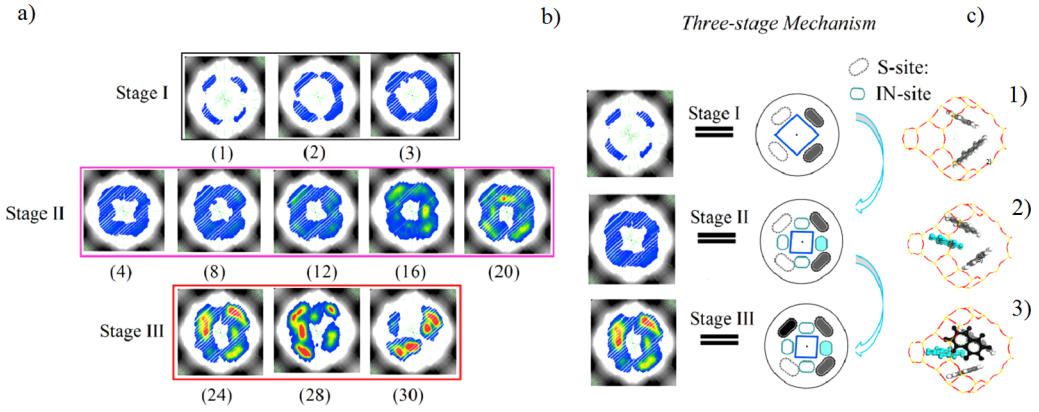

Figure 9. (a) Density contours of naphthalene molecules in 0Al, at different loadings. Numbers in parentheses are loadings in the unit of molecules/UC. Accessible and blocked places of the structure are shown as white and black. The unit of density scale is the number of adsorbate molecules per Å^3. (b) Three-stage adsorption mechanism proposed for naphthalene in FAU zeolite. (c) Low-energy configurations from the snapshots representative for three stages.

with two of the molecules occupying S sites ideally and one inserting into the SC at the center. The inserted naphthalene does not lead to a change of position of the main peak because the available space is large enough for additional naphthalene in one SC after the fitting of two naphthalene molecules. The saturation of these sites results in a loading of 24 molecules/UC, which effectively matches the previously observed value of the second I-P of $P(x)$ for naphthalene in Figure 3, signifying that the adsorption mechanism for naphthalene is a three-stage process.

Intuitively, the adsorbate distribution of naphthalene can be revealed by density contour in the plane crossing the center^{SC} shown in Figure 9a, in which loadings corresponding with different stages of the adsorption mechanism are framed together as stage I (1, 2 molecules/UC), stage II (3−24 molecules/UC), and stage III (24−30 molecules/UC). The feature of the contour is highly interesting and satisfies the aforementioned category of Figure 3. The adsorption mechanisms corresponding with the three stages are illustrated in Figure 9b.

At stage I, the naphthalene is adsorbed locally on the S sites, leaving a diamond-shaped space free of adsorbates. Although four of these positions are in the visible contour plane, only two of them can be occupied easily given the size and shape of the naphthalene as well as their ability to fit into accessible SC (as shown in Figure 9c(1)). Because of constraints imposed by the SCs, naphthalene molecules do not pack as well as smaller adsorbates in FAU. This fact is in accordance with the competitive adsorption experiment, which suggested that the packing of naphthalene in the SC of FAU zeolite is inefficient and the adsorption of the first two naphthalene molecules inside the SCs is easier than the third naphthalene molecule.[6] At stage II, naphthalenes tend to be adsorbed onto the inner side of the SC at four corners of the diamond-shaped space, which leads to a square space free of adsorbates. For one SC, this means that the third naphthalene occupies IN sites bisecting the two naphthalenes on S sites that are arranged in a V-shaped orientation (as represented by Figure 9c(2)). This configuration of naphthalene trimer has been reported by MD simulations as one of the possible lowest energy structures of the gas-phase naphthalene trimer $(C_{10}H_8)_3$ at 5−100 K.[42] This result supports our finding that each SC is gradually saturated by the trimer, which is energetically more favorable than the step-by-step saturation of S sites and IN sites. Moreover, the low-energy configuration from the snapshot, which is representative for stage II, reveals that the inserted naphthalene does not have to be equidistant from the two adsorbates at S sites (as shown in Figure 9c(2)); this condition can be rationalized as a compromise between the dispersion force that favors a face-to-face structure and the electrostatic, quadrupole−quadrupole interaction that favors a T-shaped (edge-to-face) structure.[42] At stage III, the distribution of naphthalene tends to be much more localized than lower loadings; interestingly, neither reorganizing of revealed adsorption sites nor revealing of new adsorption sites can be recognized in the density contour. Upon closer inspection of many low-energy snapshots at saturated loadings, we find that the newly adsorbed naphthalene tends to be located on the S site, while not exactly "ideally" located. As shown in Figures 9c(3) and 10,

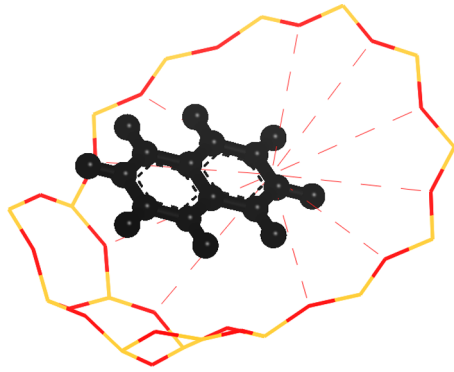

Figure 10. Low-energy configuration of the naphthalene molecule representative for stage III.

the black naphthalene represents newly adsorbed naphthalene on the S site (more or less inserted into the 12-T ring) after the saturation of IN sites. If this is the case, then the first peak of RDFs of the COM-12^C representing the utilization of the 12-T ring should be increased and broadened to a certain extent, which is contrary to the findings for the insertion mechanism. As shown in Figure 11, the first peak of COM-12^C decreases slightly at loadings below 24 molecules/UC and then increases significantly at higher loadings.

So far, the three-stage mechanism composed of ideal adsorption, insertion adsorption, and overideal adsorption can

DOI: 10.1021/acsami.5b00399
ACS Appl. Mater. Interfaces 2015, 7, 10190−10200

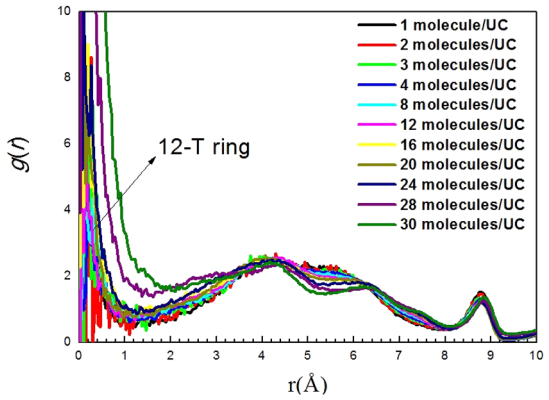

Figure 11. RDFs of COM−12^{C} for naphthalene on 0Al at various loadings.

be proposed for naphthalene, with two I-P corresponding with 3 and 24 molecules/UC. The so-called overideal adsorption is labeled based on the configuration of the last few naphthalene molecules contributing to the maximum adsorption capacity, which occupied the S sites nonideally with their long axes pointing to the 12^{C}.

3.5. Interaction Energies. Based on the revealed adsorption mechanisms, the loading dependence of the energetic property of adsorption for the aromatics in the 0Al model can be improved significantly. The isosteric heats of adsorption of benzene (Q) are calculated as follows:

$$Q = RT - \left(\frac{\partial(U_{ad} - U_{intra})}{\partial N_{ad}}\right)_{V,T}$$

where R is the gas constant, N_{ad} is the loading of benzene, U_{ad} is determined by summing all interactions between pairs of adsorbate molecules ($U_{ads\text{-}ads}$) as well as all adsorbate interactions with the zeolite framework ($U_{ads\text{-}zeo}$), and U_{intra} is the intramolecular energy of the adsorbate molecules. Thus, a positive correlation is observed between Q and the absolute value of U_{ad}.

Figure 12a shows the Q of benzene, toluene, styrene, *o*-, *m*-, and *p*-xylene, TMB, and naphthalene on the 0Al model at 298 K. Two dominant features of Q are revealed. First, the Q increases with increasing kinetic diameters of adsorbates over the entire loading range, that is, in the sequence benzene < toluene < C8 (styrene and *o*-, *m*-, and *p*-xylene) < TMB < naphthalene. Second, an increase in Q of more than 6 kcal/mol upon loading, with a three-stage profile resembling a previous finding for benzene/HY zeolites (Si:Al = 2.34−∞),[43] is found for all of the adsorbates in 0Al. More specifically, two changing points separate the data of Q into three ranges (low, medium, and high loading) with $R^2 > 0.99$. The first one is distinguished by blue diagonal lines at 8 molecules/UC and the second is distinguished by red staggered grids that correspond to the I-P illustrated earlier in this paper.

To elaborate on the reason for these changes, the total host−guest interaction energies (U_{ad}) are decomposed into $U_{ads\text{-}zeo}$ and $U_{ads\text{-}ads}$ components (Figure 12b,c). When coverage is increased, decreased $U_{ads\text{-}zeo}$ at low loadings reveals heterogeneity of adsorption sites.[15] At medium and high loading ranges, the $U_{ads\text{-}zeo}$ almost remains constant in magnitude for all adsorbates. However, in consideration of the change of the adsorption mechanism (from ideal adsorption referring to adsorption ideally on energetically favorable S sites to insertion adsorption characterized by the capture of less stable IN sites) for the monoaromatics at the I-P, the flat heat profile observed

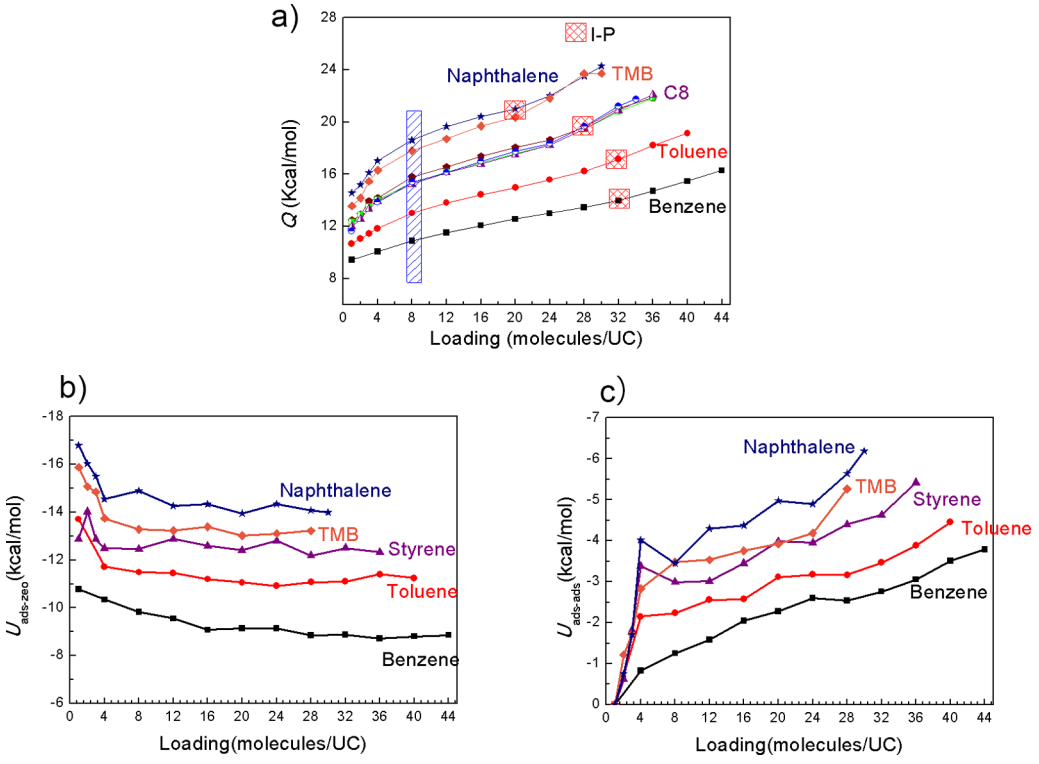

Figure 12. (a) Calculated Q of adsorbates at room temperature in the 0Al model. Calculated adsorption energy (U_{ad}) decomposed into (b) $U_{ads\text{-}zeo}$ and (c) $U_{ads\text{-}ads}$ components for benzene, toluene, C8, TMB, and naphthalene.

DOI: 10.1021/acsami.5b00399
ACS Appl. Mater. Interfaces 2015, 7, 10190−10200

could not be interpreted as the adsorption of molecules on a set of equivalent and independent sites.[24] Instead, the observed constancy of $U_{ads\text{-}zeo}$ is due to internal compensation of two competing effects. On one hand, the capture of unfavorable IN sites results in decreasing $U_{ads\text{-}zeo}$; on the other hand, the inserted molecules that push the adsorbates on ideal sites closer to the framework lead to attractive $U_{ads\text{-}zeo}$.

We can consider the evolution of $U_{ads\text{-}ads}$ as the main reason for the origin of the change of slopes for Q versus the loading curves in Figure 12a because the curve of $U_{ads\text{-}ads}$ exhibits a similar three-stage pattern with Q versus loading, and the $\Delta U_{ads\text{-}ads}$ (positive) is larger than the absolute value of $\Delta U_{ads\text{-}zeo}$ (negative) in the entire loading range. The sharper increase of Q with increasing loading at the low loading range clearly stems from the emergence of $U_{ads\text{-}ads}$. At the high loading range, the adsorbates start to occupy the IN sites, which result in a closer distance between adsorbed molecules, thereby leading to a sharper increase of $U_{ads\text{-}ads}$ and Q with loading. The standpoint of the closer location of adsorbed molecule at high loading range can be confirmed by RDFs of COM−COM in Figures 4a and 8a, showing that well-defined shoulder peaks corresponding to IN sites increase with loading at 4−5 Å. In summary, the loading-dependent isosteric heat could be divided into three ranges, and the two change points correspond with the emergence of $U_{ads\text{-}ads}$ and the change of adsorption mechanism of adsorbates.

4. CONCLUSIONS

This study reports the adsorption of aromatics in FAU zeolite, which is the first case concerning the basic law of adsorption mechanism at all loadings. The change of adsorption mechanism from "ideal adsorption" to "insertion adsorption" is observed for toluene, styrene, *o*-, *m*-, and *p*-xylene, and TMB, which is believed to be a general characteristic of adsorption in FAU zeolites for monoaromatics. In addition, the smaller aromatic molecules reach the inflection point (I-P) at higher concentrations, roughly estimated as 32, 32, 28, 28, 20, and 3 for benzene, toluene, styrene, *o*-, *m*-, and *p*-xylene, TMB, and naphthalene, respectively. Thus, packing is related to the number of C atoms per unit cell corresponding to the I-P of adsorbate loading ($C_{I\text{-}P}$). It is revealed to be a valid characterization factor of packing efficiency of monoaromatics in the FAU zeolite. Specifically, the packing efficiency increases first for small aromatics ($C_{I\text{-}P}$(toluene) > $C_{I\text{-}P}$(benzene)), remains constant for C8 aromatics, and finally decreases with the C number of adsorbates. The reason for the two turning points is utilization of the 12-T ring and size effect, respectively. In addition, the packing efficiency of TMB is only slightly lower than that of benzene, which highlights the significant role that 12-T ring plays in diminishing the size effect. This condition deviates from the general rule of packing in zeolites, which states that fewer branched aromatics are packed more efficiently for aromatics with a similar kinetic diameter.[21]

For diaromatic naphthalene, the three-stage mechanism is proposed, which consists of the third stage of "overideal adsorption" in addition to the ideal and insertion adsorption stages. The so-called overideal adsorption is labeled because, at loadings approaching saturation, the naphthalene molecules start to occupy the S site again but nonideally, thereby leading to a more localized feature of the adsorbates. In contrast to the monoaromatics, which can occupy only the insertion site after the saturation of S sites, the naphthalene molecule tends to insert into the supercage after the first two adsorbates because of a difference in packing efficiency between the aromatics and the high stability of the trimer. The loading dependence of the energetic property of adsorption for the aromatics in the 0Al model is improved significantly by the proposed adsorption mechanism.

■ ASSOCIATED CONTENT

Supporting Information

Detailed information on partial charges of atoms for both adsorbates and the zeolite model and results for styrene, *o*-xylene, and TMD, figures showing density contours, representative trajectories, and RDFs, and a table listing partial charges. The Supporting Information is available free of charge on the ACS Publications website at DOI: 10.1021/acsami.5b00399.

■ AUTHOR INFORMATION

Corresponding Author

*Tel.: (+)86-10-89739078. Fax: (+) 86-10-69724721. E-mail: liangzhao@cup.edu.cn.

Author Contributions

[§]H.Z. and L.Z. contributed equally to this work.

Notes

The authors declare no competing financial interest.

■ ACKNOWLEDGMENTS

We acknowledge the financial support of TOTAL S.A., Scientific Division, Paris. This study was also sponsored by the National Natural Science Foundation of China (Grant Nos. 21176253, 21476260, 21036008, 21236009, and U1162204).

■ ABBREVIATIONS

12^C = center of the 12-T ring
12-T ring = 12-membered window
C1 = C atoms forming aromatic ring
C2 = C atoms at the end of the branch chain
$C_{I\text{-}P}$ = C atoms per unit cell corresponding to the I-P
$center^{SC}$ = center of the SC
COM = center of mass
d = kinetic diameters
FAU = faujasite
IN site = insertion site near the $center^{SC}$
I-P = inflection point of loading
molecule/UC = molecule per unit cell
Q = heats of adsorption
S site = conventional site in the SC near the zeolite framework
SC = supercage
TMB = 1,3,5-trimethylbenzene
$U_{ad} = U_{ads\text{-}ads} + U_{ads\text{-}zeo}$
$U_{ads\text{-}ads}$ = all interactions between pairs of adsorbate molecules
$U_{ads\text{-}zeo}$ = all adsorbate interactions with the zeolite framework
U_{intra} = intramolecular energy of the adsorbate molecules

■ REFERENCES

(1) Hattori, H. Heterogeneous Basic Catalysis. *Chem. Rev.* **1995**, *95*, 537−558.
(2) Occelli, M. L. *Fluid catalytic cracking 2*; American Chemical Society: Washington, DC, USA, 1991.

DOI: 10.1021/acsami.5b00399
ACS Appl. Mater. Interfaces 2015, 7, 10190−10200

(3) Jentoft, F. C.; Kröhnert, J.; Subbotina, I. R.; Kazansky, V. B. Quantitative Analysis of IR Intensities of Alkanes Adsorbed on Solid Acid Catalysts. *J. Phys. Chem. C* **2013**, *117*, 5873−5881.
(4) Krishna, R.; Calero, S.; Smit, B. Investigation of Entropy Effects During Sorption of Mixtures of Alkanes in MFI Zeolite. *Chem. Eng. J.* **2002**, *88*, 81−94.
(5) Jiang, Y.; Huang, J.; Hunger, M. Effect of Reactant Density Inside Supercages of Zeolite La, Na-Y on the Mechanism of the Ethylbenzene Conversion. *Catal. Today* **2011**, *164*, 119−123.
(6) Daems, I.; Leflaive, P.; Méthivier, A.; Denayer, J. F. M.; Baron, G. V. Size and Packing Related Adsorption Effects in the Liquid Phase Adsorption of Aromatics and Alkenes on FAU Type Zeolites. *Stud. Surf. Sci. Catal.* **2005**, *158*, 1177−1184.
(7) Schaefer, D. J.; Favre, D. E.; Wilhelm, M.; Weigel, S. J.; Chmelka, B. F. Site-Hopping Dynamics of Benzene Adsorbed on Ca-LSX Zeolite Studied by Solid-State Exchange 13C NMR. *J. Am. Chem. Soc.* **1997**, *119*, 9252−9267.
(8) Zeng, Y.; Ju, S.; Xing, W.; Chen, C. Computer Simulation of Benzene Adsorbed in All-silica Y and NaY Zeolites. *Ind. Eng. Chem. Res.* **2007**, *46*, 242−248.
(9) Laborde-Boutet, C.; Joly, G.; Nicolaos, A.; Thomas, M.; Magnoux, P. Selectivity of Thiophene/Toluene Competitive Adsorptions onto Zeolites. Influence of the Alkali Metal Cation in FAU(Y). *Ind. Eng. Chem. Res.* **2006**, *45*, 8111−8116.
(10) Klein, H.; Fuess, H.; Schrimpf, G. Mobility of Aromatic Molecules in Zeolite NaY by Molecular Dynamics Simulation. *J. Phys. Chem.* **1996**, *100*, 11101−11112.
(11) Keffer, D.; Davis, H. T.; McCormick, A. The Effect of Nanopore Shape on the Structure and Isotherms of Adsorbed Fluids. *Adsorption* **1996**, *2*, 9−21.
(12) Song, L.; Sun, Z.; Duan, L.; Gui, J.; McDougall, G. S. Adsorption and Diffusion Properties of Hydrocarbons in Zeolites. *Microporous Mesoporous Mater.* **2007**, *104*, 115−128.
(13) Zheng, H. M.; Zhao, L.; Yang, Q.; Ji, J. J.; Gao, J. S. Insight into the Adsorption Mechanism of Benzene in HY Zeolites: the Effect of Loading. *J. Catal.* **2015**, submitted for publication.
(14) Lee, K.-H.; Ha, B.-H.; Lee, Y.-W. Catalytic Cracking of Vacuum Gas Oil over the Modified Mordenites and Y-Type Zeolites Mixed with Alumina. *Ind. Eng. Chem. Res.* **1998**, *37*, 1761−1768.
(15) Fitch, A.; Jobic, H.; Renouprez, A. Localization of Benzene in Sodium-Y-zeolite by Powder Neutron Diffraction. *J. Phys. Chem.* **1986**, *90*, 1311−1318.
(16) Zheng, H. M.; Zhao, L.; Yang, Q.; Gao, J. S.; Shen, B. J.; Xu, C. M. Influence of Framework Protons on the Adsorption Sites of the Benzene/HY System. *Ind. Eng. Chem. Res.* **2014**, *53*, 13610−13617.
(17) Van der Perre, S.; Van Assche, T.; Bozbiyik, B.; Lannoeye, J.; De Vos, D. E.; Baron, G. V.; Denayer, J. F. M. Adsorptive Characterization of the ZIF-68 Metal-Organic Framework: A Complex Structure with Amphiphilic Properties. *Langmuir* **2014**, *30*, 8416−8424.
(18) Lue, S. J.; Su, I. M.; Lee, D.-T.; Chen, H.-Y.; Shih, C.-M.; Hu, C.-C.; Jean, Y. C.; Lai, J.-Y. Correlation between Free-Volume Properties and Pervaporative Flux of Polyurethane−Zeolite Composites on Organic Solvent Mixtures. *J. Phys. Chem. B* **2011**, *115*, 2947−2958.
(19) Yu, M.; Noble, R. D.; Falconer, J. L. Zeolite Membranes: Microstructure Characterization and Permeation Mechanisms. *Acc. Chem. Res.* **2011**, *44*, 1196−1206.
(20) Yu, M.; Falconer, J. L.; Noble, R. D. Characterizing Nonzeolitic Pores in MFI Membranes. *Ind. Eng. Chem. Res.* **2008**, *47*, 3943−3948.
(21) Gopal, S.; Zhang, W.; Smirniotis, P. G. Comparison of Hydroisomerization and Hydrocracking Reactions of Normal and Branched Octanes over USY and ZSM-12 Catalysts. *Ind. Eng. Chem. Res.* **2003**, *43*, 2950−2956.
(22) Li, G.; Wang, Z. Naphthalene-Based Microporous Polyimides: Adsorption Behavior of CO_2 and Toxic Organic Vapors and Their Separation from Other Gases. *J. Phys. Chem. C* **2013**, *117*, 24428−24437.
(23) Sun, H. COMPASS: An ab Initio Force-Field Optimized for Condensed-Phase Applications Overview with Details on Alkane and Benzene Compounds. *J. Phys. Chem. B* **1998**, *102*, 7338−7364.
(24) Mellot, C. F.; Cheetham, A. K.; Harms, S.; Savitz, S.; Gorte, R. J.; Myers, A. L. Calorimetric and Computational Studies of Chlorocarbon Adsorption in Zeolites. *J. Am. Chem. Soc.* **1998**, *120*, 5788−5792.
(25) Arı, M. U.; Ahunbay, M. G.; Yurtsever, M.; Erdem-Şenatalar, A. Molecular Dynamics Simulation of Water Diffusion in MFI-type Zeolites. *J. Phys. Chem. B* **2009**, *113*, 8073−8079.
(26) Fleys, M.; Thompson, R. W. Monte Carlo Simulations of Water Adsorption Isotherms in Silicalite and Dealuminated Zeolite Y. *J. Chem. Theory Comput.* **2005**, *1*, 453−458.
(27) Yang, J. Z.; Liu, Q. L.; Wang, H. T. Analyzing Adsorption and Diffusion Behaviors of Ethanol/Water Through Silicalite Membranes by Molecular Simulation. *J. Membr. Sci.* **2007**, *291*, 1−9.
(28) Zhao, L.; Zhai, D.; Liu, B.; Liu, Z.; Xu, C.; Wei, W.; Chen, Y.; Gao, J. Grand Canonical Monte Carlo Simulations for Energy Gases on PIM-1 Polymer and Silicalite-1. *Chem. Eng. Sci.* **2012**, *68*, 101−107.
(29) Wu, J. Y.; Liu, Q. L.; Xiong, Y.; Zhu, A. M.; Chen, Y. Molecular Simulation of Water/Alcohol Mixtures' Adsorption and Diffusion in Zeolite 4A Membranes. *J. Phys. Chem. B* **2009**, *113*, 4267−4274.
(30) Fermeglia, M.; Pricl, S. Prediction of Phase Equilibria for Binary Mixtures by Molecular Modeling. *AIChE J.* **2001**, *47*, 2371−2382.
(31) Jirapongphan, S. S.; Warzywoda, J.; Budil, D. E.; Sacco, A. The Role of Sorbate in the Determination of Preferential Adsorption Sites in Zeolite HY: A Theoretical Study. *Microporous Mesoporous Mater.* **2007**, *103*, 280−283.
(32) Jousse, F.; Auerbach, S. M.; Vercauteren, D. P. Adsorption Sites and Diffusion Rates of Benzene in HY Zeolite by Force Field Based Simulations. *J. Phys. Chem. B* **2000**, *104*, 2360−2370.
(33) Mészár, Z. E.; Hantal, G.; Picaud, S.; Jedlovszky, P. Adsorption of Aromatic Hydrocarbon Molecules at the Surface of Ice, As Seen by Grand Canonical Monte Carlo Simulation. *J. Phys. Chem. C* **2013**, *117*, 6719−6729.
(34) Beck, L. W.; Xu, T.; Nicholas, J. B.; Haw, J. F. Kinetic NMR and Density Functional Study of Benzene H/D Exchange in Zeolites, the Most Simple Aromatic Substitution. *J. Am. Chem. Soc.* **1995**, *117*, 11594−11595.
(35) Smit, B.; Siepmann, J. I. Simulating the Adsorption of Alkanes in Zeolites. *Science* **1994**, *264*, 1118−1120.
(36) Tao, Y.; Xue, Q.; Liu, Z.; Shan, M.; Ling, C.; Wu, T.; Li, X. Tunable Hydrogen Separation in Porous Graphene Membrane: First-Principle and Molecular Dynamic Simulation. *ACS Appl. Mater. Interfaces* **2014**, *6*, 8048−8058.
(37) Si, L.; Guo, D.; Xie, G.; Luo, J. Mechanical Properties and Interface Characteristics of Nanoporous Low-k Materials. *ACS Appl. Mater. Interfaces* **2014**, *6*, 13850−13858.
(38) Bai, P.; Siepmann, J. I.; Deem, M. W. Adsorption of Glucose into Zeolite Beta from Aqueous Solution. *AIChE J.* **2013**, *59*, 3523−3529.
(39) Brémard, C.; Ginestet, G.; Le Maire, M. Sorption Sites, Energetics, and Reactions of Molybdenum Hexacarbonyl and Benzene Cosorbed in Faujasitic Zeolites. *J. Am. Chem. Soc.* **1996**, *118*, 12724−12734.
(40) Takahashi, A.; Yang, F. H.; Yang, R. T. New Sorbents for Desulfurization by π-Complexation: Thiophene/Benzene Adsorption. *Ind. Eng. Chem. Res.* **2002**, *41*, 2487−2496.
(41) Yu, M.; Hunter, J. T.; Falconer, J. L.; Noble, R. D. Adsorption of Benzene Mixtures on Silicalite-1 and NaX Zeolites. *Microporous Mesoporous Mater.* **2006**, *96*, 376−385.
(42) Benharash, P.; Gleason, M. J.; Felker, P. M. Rotational Coherence Spectroscopy and Structure of Naphthalene Trimer. *J. Phys. Chem. A* **1999**, *103*, 1442−1446.
(43) Zheng, H. M.; Zhao, L.; Ji, J. J.; Yang, Q.; Gao, J. S. Molecular Origin of Decreased Diffusivity with Loading for Benzene/HY. *AIChE J.* **2015**, submitted for publication.

DOI: 10.1021/acsami.5b00399
ACS Appl. Mater. Interfaces 2015, 7, 10190−10200